Supporting Information

Cocrystallisation of caffeine:1-hydroxy-2-naphthoic acid at polarized oil-water interfaces

Magdalena Kaliszczak,[1] Pierrick Durand,[2] Emmanuel Wenger,[2] Manuel Dossot,[1] Franca Jones,[3] Damien W. M. Arrigan,[3*] Grégoire Herzog[1*]

[1:] Université de Lorraine, CNRS, LCPME, F-54000 Nancy, France
[2:] Université de Lorraine, CNRS, CRM[2], F-54000 Nancy, France
[3:]School of Molecular and Life Sciences, Curtin University, GPO Box U1987, Perth, Western Australia 6845, Australia

*: D.Arrigan@curtin.edu.au; gregoire.herzog@univ-lorraine.fr

Table of contents

Materials and Methods

Chemicals

The organic phase was 1, 2-dichloroethane (DCE, > 99.5%) from Sigma-Aldrich. The aqueous

phase electrolyte was 10 mM lithium chloride (LiCl, ≥ 99.0%, Sigma-Aldrich). The pH of the aqueous phase was adjusted with hydrochloric acid (HCl, 1 molL^{-1}, VWR Chemicals). Studied drugs: caffeine powder (Caff, Lab Grade, Fisher Scientific), 1-hydroxy-2-naphthoic acid (1H2N, 99.0%, Aldrich). Bis(triphenylphosphoranylidene)ammonium chloride (BACl, Sigma-Aldrich, 97%) and potassium tetrakis(4-chlorophenyl) borate (KTPBCl, Sigma-Aldrich, ≥ 98.0%) were used to prepare the organic phase electrolyte bis(triphenylphosphoranylidene)ammonium tetrakis(4-chlorophenyl) borate (BATPBCl) via a metathesis reaction according to the protocol[1]. Tetrapropylammonium chloride (TPA, 98%, Aldrich) were used as reference to measure the half-wave potential.KTPBCl and BACl were used to chemically polarize the interface. Chlorotrimethylsilane (≥ 98.0% (GC), Sigma-Aldrich) was used for silanization.

Control of the interfacial potential difference by chemical polarisation

The following salts LiCl, KTPBCl, BACl were dissolved in the aqueous and organic phases according to the Scheme 1 to chemically polarise the interface. Each ion present in the system is distributed in equilibrium between the water and organic phase resulting in change of the interfacial potential $(\Delta_o^w\phi)$[3,4].

Scheme S1. Experimental set up presenting chemical polarisation of the interface. BACl – Bis(triphenylphosphoranylidene)ammonium chloride; KTPBCl – potassium tetrakis(4-ch

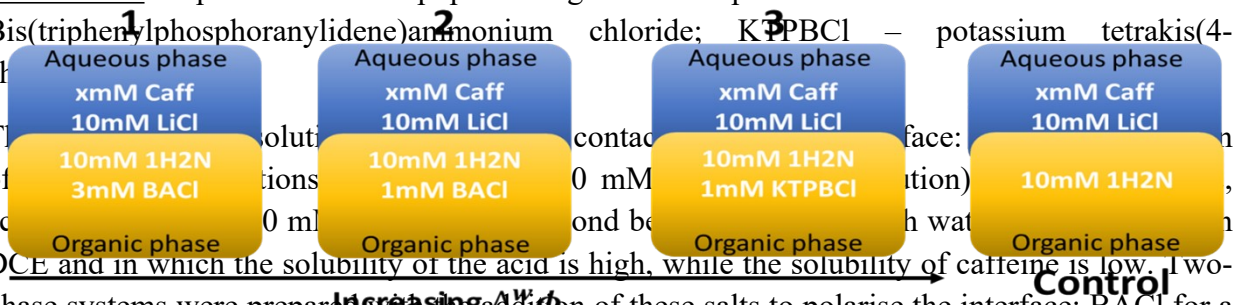

Th soluti contac face: n of tions 0 mM tion) , ac 0 ml ond be h wat n DCE and in which the solubility of the acid is high, while the solubility of caffeine is low. Two-phase systems were prepared with the addition of these salts to polarise the interface: BACl for a low polarisation and KTPBCl for high polarisation. This potential difference was verified by the open circuit potential (OCP) measurements: OCPs were -2.80 V (vial 1), 0.09 V (vial 2) and 0.57 V (vial 3). A fourth biphasic system without polarisation was prepared as a control sample. The aqueous phase was added drop wise to the organic phase to form an interface and was left overnight. The volume of both phases was 1.5 mL. The cocrystals were collected and any residual aqueous or organic solvent was left to evaporate. The vials were previously silanised to flatten the interface and increase the contact surface by filling the glassware at the bottom half with chlorotrimethylsilane and left to evaporate at room temperature under the fume hood.

Control of the interfacial potential difference by potentiostat

The potential difference across the water/1,2-dichloroethane interface was controlled with an Autolab potentiostat PGSTAT302N or PGSTAT-100 controlled by NOVA software (Version 1.11). All measurements were performed in a four-electrode glass cell with an interface area of ~1.13 cm^2. Platinum mesh was used as the counter electrodes and Ag/AgCl wire as reference electrodes in both phases. To avoid exposure on the aqueous phase, the organic phase counter electrode was previously covered with borosilicate glass. The organic phase reference electrode

was immersed in its aqueous reference solution of LiCl and BACl. All measurements were carried out at room temperature (25 °C). The half-wave potentials were referred to the half-wave potential of TPA^+ ($\Delta_o^w\phi_{TPA^+}^0 = -0.093$ V)[2] and obtained by adding a predetermined concentration of the chloride salt of TPA+ to the cell for each experiment. Examined compounds were dissolved in aqueous and/or organic phase electrolyte solution before filling the cell. The volume added to the cell in each phase was always exactly 2.5 mL.

Scheme S2. The electrochemical cell configurations.

Electrochemical cell 1:

Electrochemical cell 2:

Raman Spectroscopy

Experimental Raman scattering spectra were collected at 295 K on a Renishaw inVia™ Qontor® confocal micro[illegible] of 1200 grooves per mm, a CCD [illegible] quisition units 70 cm^{-1}. The laser [illegible] working distance of 7 mm and a numerical aperture of 0.90. Excitation irradiance at the sample was about 1000 $W.cm^{-2}$, which avoided any laser heating of the sample. Exposure time was 2 seconds and 5 spectra were averaged for increasing signal-to-noise ratio. Raman spectra were collected in step scan mode from 70 to 3200 or 3600 cm^{-1} depending on the sample. The final spectral resolution was closed to 3 cm^{-1} using this grating. At least 10 spectra were collected for each sample and we checked that the spectra were identical, indicating that the samples were quite homogeneous.

Density-functional theory (DFT) calculations were made by the method of the DFT calculation at B3LYP 6311G++ (3d, 3p) level in gas phase. They were used to optimize the geometry of caffeine and 1H2N molecules, and the cocrystal involving a 1:1 complex between these two components. Vibrational spectra were calculated once the geometry was optimized, and no negative frequency was obtained, indicating a good convergence of the calculations. The aim was to compare the Raman active vibrational modes obtained experimentally and by a computational quantum mechanical modelling method. DFT computation and correction of the calculated vibrational wavenumbers by the following quadratic scaling function:[1]

$$\bar{\sigma}_{scaled} = -0.0000104\bar{\sigma}_{calc}^{2} + 0.9894\bar{\sigma}_{calc}$$

Where $\bar{\sigma}_{scaled}$ is the corrected Raman shift in cm^{-1}, and $\bar{\sigma}_{calc}$ is the calculated DFT Raman shift.

The following figures report the comparison between experimental and theoretical Raman spectra for caffeine, 1H2N and the 1/1 cocrystal of these two molecules. Associated tables report the frequencies and the normalized Raman intensities, as well as the most important assignments for the two isolated molecules (caffeine and 1H2N). For caffeine, the assignment used the numbering

of atoms indicated in Figure S9. For the cocrystal structure, we have only assigned the most important peaks featuring the frequencies strongly modified by hydrogen bonds. One can see that the theoretical spectra are in very good agreement with the experimental ones for the frequencies. It is less true concerning the Raman intensities, but this is well known for DFT calculations. Nevertheless, the agreement is acceptable.

X-ray Diffraction

The PXRD measurements were performed using a Panalytical X'Pert Pro diffractometer equipped with a Cu tube, a Ge (111) incident-beam monochromator (Kα1 = 1.5406 Å), 0.02 rad Soller slits, programmable divergence and anti-scatter slits, the irradiated area was fixed to 10mm x 10mm and an X'Celerator fast detector. The X'Celerator detector was used as "scanning line detector (1D)" with 2.122° active length. The resulting powder was characterized on a 200 μm thick zero background X-ray holder because of relatively small amounts of powder (10 – 20 mg). Data collection was carried out in the scattering angle range 3 – 50° with a 0.0167° step over 4 hours. Powder X-Ray diffractograms were recorded in reflection mode (Bragg Brentano θ-2θ), and their patterns were simulated for the 2 phases, using their known phase structure. A semi-quantitative model based on intensity was used to determine the composition of the phase mixture.

The single crystal X-ray diffraction (SCXRD) measurements were performed using a Rigaku Oxford Diffraction 4-circles SuperNova diffractometer with a microfocus Molybdenum anode X-ray source (wavelength Mo ($K\alpha_1$, α_2) = 0.71073 Å) and an Atlas CCD detector. The cell parameters determination was carried out at room temperature.

Scanning electron microscopy

Scanning electron microscopy micrographs were obtained using a JEOL JCM-6000 (acceleration voltage of 15 kV).

Complementary results

Crystallisation of Caffeine:1H2N at the polarised liquid-liquid interface

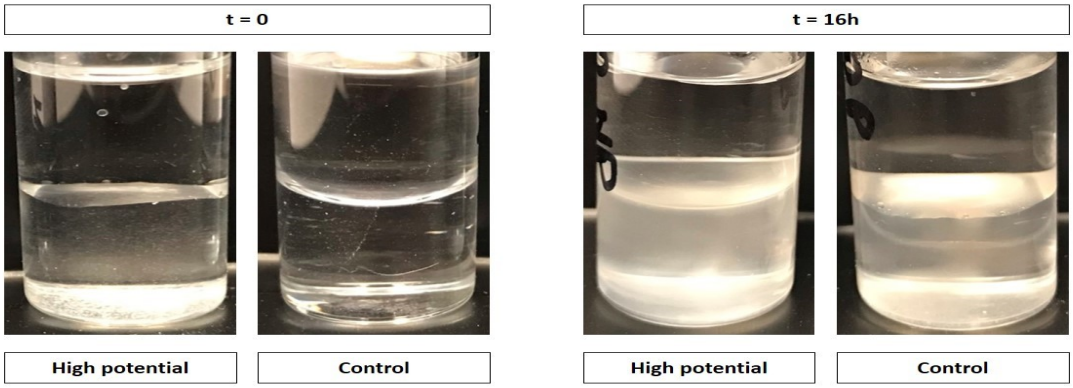

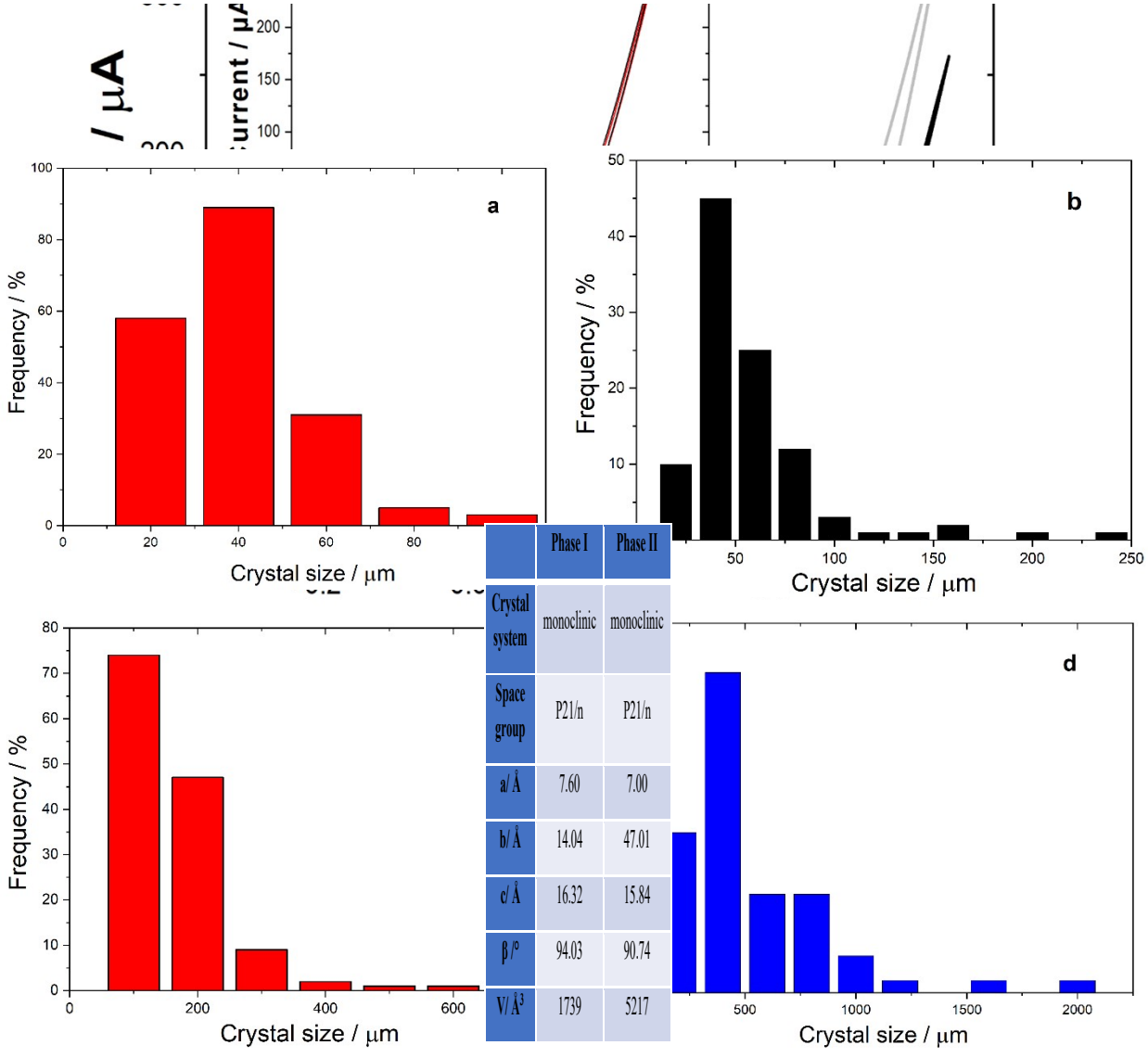

	Phase I	Phase II
Crystal system	monoclinic	monoclinic
Space group	P21/n	P21/n
a/ Å	7.60	7.00
b/ Å	14.04	47.01
c/ Å	16.32	15.84
β /°	94.03	90.74
V/ Å^3	1739	5217

Powder X-ray Diffraction

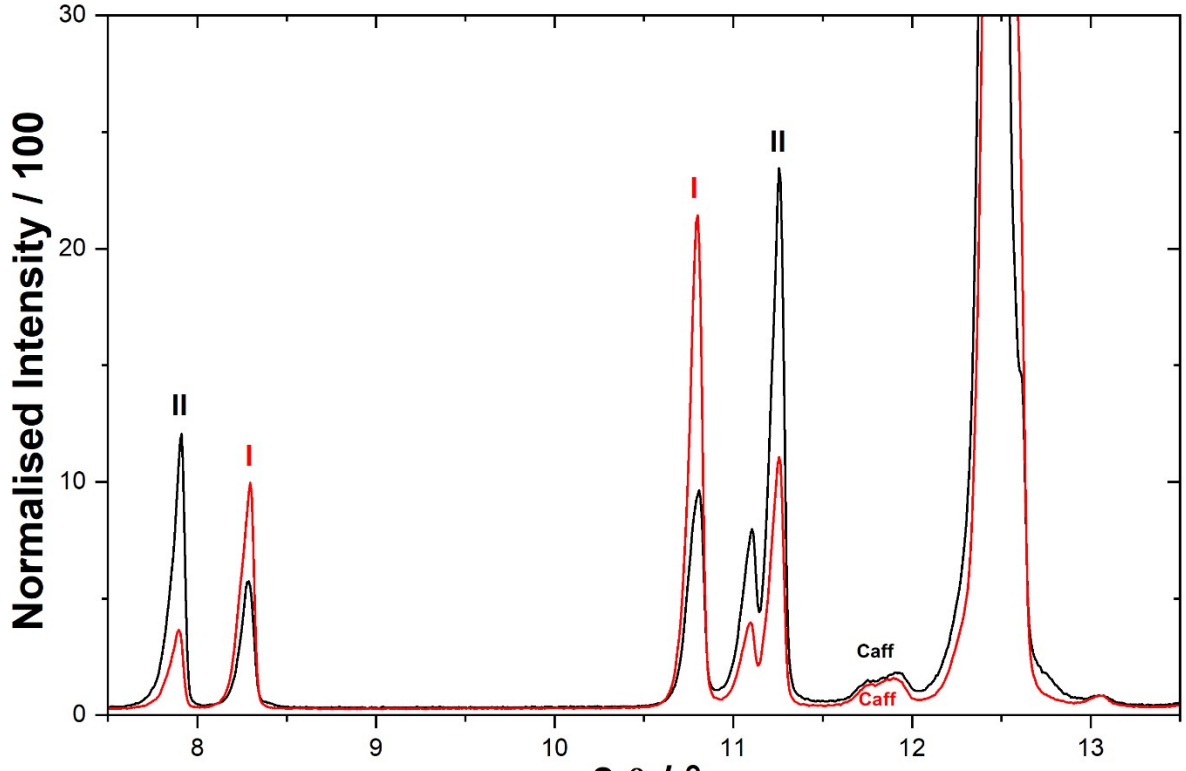

Raman Spectroscopy

These peaks are consistent with data collected by DFT calculations: the differences in the intensity are negligible and the positions of the characteristic bands correspond to practically identical frequencies. We observe a relatively larger inconsistency between the calculated frequencies and the experimental vibrations for caffeine and 1H2N (Fig S7). However, the characteristic band of caffeine and 1H2N obtained by the experiment agree with those reported in the literature[8,9]. These differences between the experimental and calculated spectra may be explained by the fact that the calculations did not consider intermolecular interactions and were carried out for the single molecule in gas phase[10]. For the cocrystals, where the H-bonds between the two molecules are calculated, the peaks between the experimental and calculated spectra are in better agreement.

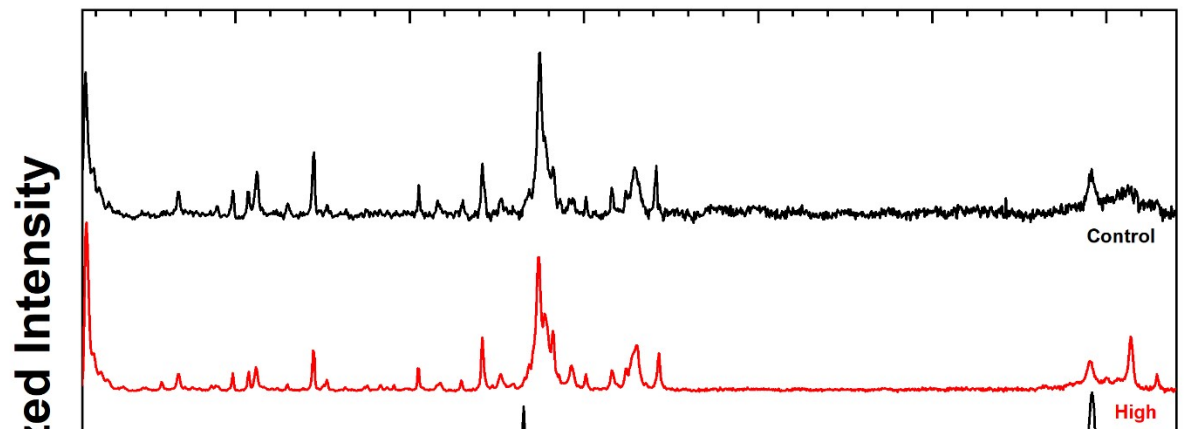

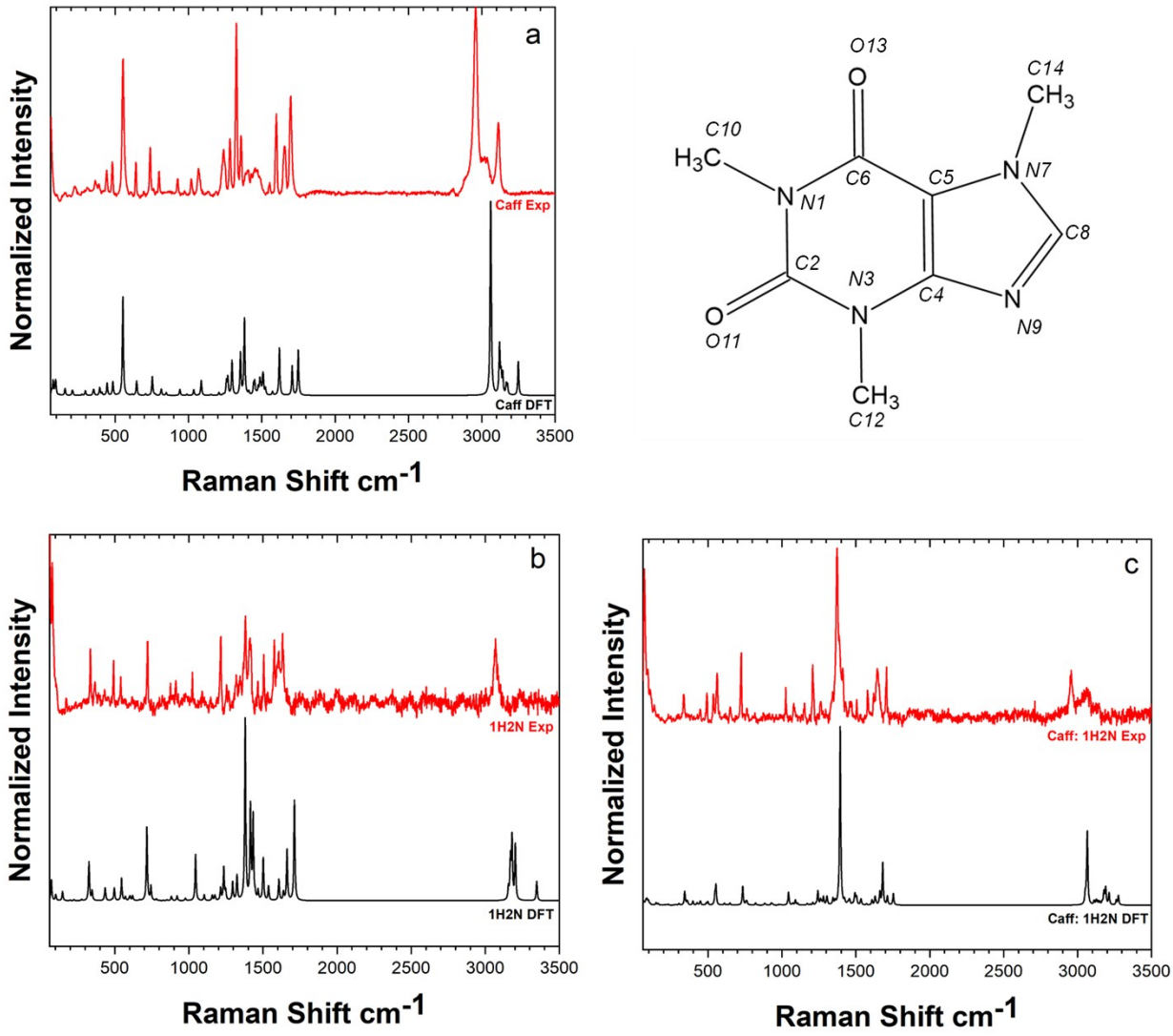

Figure S8: Experimental (red) and DFT calculated (black) Raman spectra for (a) Caff, (b) 1H2N, and (c) Caff: 1H2N (obtained at high polarization). Caffeine structure is also given along with the numbering of carbons atoms used in Table S3.

Table S3: Assignment for the most characteristic vibrational bands of caffeine[11].

Experimental Raman shifts	Experimental Raman Normalized Intensity	DFT calculated and corrected Raman shifts	DFT Raman Normalized Intensity	Assignement
446	0.143	438	0.064	CH_3 sym. bend + CH_3 rock
486	0.228	477	0.072	Imidazole ring def + O=C–N def + CH bend
557	0.81	544	0.508	CH bend + CH_3 sym. bend + CH_3 rock
646	0.211	636	0.075	midazole ring def + O=C–N def + CH_3 sym. bend
742	0.261	740	0.098	Imidazole ring def + CH_3 sym. bend + CH_3 rock
803	0.149	802	0.028	Imidazole ring def + C=O def + CH_3 rock
930	0.105	923	0.031	Imidazole + CH_3 rock
1026	0.097	1014	0.028	CH_3 rock + C–N stretch + C–N bend
1073	0.15	1064	0.077	H–C=N bending
1243	0.271	1230	0.087	H–C=N bending
1250 (shoulder)	0.217	1238	0.101	C–N stretch
1287	0.361	1266	0.182	C2–N3 sym. str + CH_3 rock
1332	1	1322	0.226	Imidazole trigonal ring stretch
1363	0.374	1346	0.386	C–N str + CH_3 sym. Bending
1410 (broad)	0.178	1410	0.078	CH_3 sym. bend + C14–N7 sym. str
1433 (broad)	0.158	1434	0.147	CH_3 twisting
1470 (broad)	0.184	1469	0.121	CH_3 sym. bending
1556	0.107	1531	0.021	CH_3 sym. bend + CH_3 bend + C–N stretch
1602	0.474	1576	0.245	C=C sym. str + C–N sym. str + CH_3 sym. bend
1658	0.314	1658	0.153	Out-of-phase C=O stretch + C=C sym. Stretch
1701	0.546	1699	0.232	In-phase C=O stretch
2960 (broad)	0.685	2931	1	CH_3 sym. stretch
3030 (broad. multiple)	0.175	2986	0.275	CH_3 asym. stretch
		2996	0.151	CH_3 asym. stretch
		3006	0.128	CH_3 asym. stretch
		3027	0.0674	CH_3 asym. stretch
		3036	0.064	CH_3 asym. stretch
3117	0.301	3103	0.172	imidazole C-H stretch

Table S4: Assignment for the most characteristic vibrational bands of 1-hydroxy-2-naphthoic acid[9].

Experimental Raman shifts	Experimental Raman Normalized Intensity	DFT calculated and corrected Raman shifts	DFT Raman Normalized Intensity	Assignement
340	0,523	321	0,214	naphtalene squeletal in plane deformation
370	0,226	342	0,06	
439	0,121	428	0,071	
498	0,415	490	0,064	
546	0,273	538	0,124	naphtalene squeletal in plane deformation
620	0,158	592	0,03	
725	0,694	703	0,403	
753	0,163	731	0,086	
881	0,159	865	0,022	
917	0,219	902	0,027	
1029	0,385	1023	0,253	ring breathing mode
1098	0,158	1080	0,032	
1157	0,161	1151	0,027	
1190	0,14	1186	0,075	
1219	0,768	1206	0,188	naphtalene CCH bend + C=C stretch + C-O-H bend
1262	0,345	1265	0,104	
1274	0,274	1290	0,142	naphtalene CCH bend and C=C stretch
1326 (broad)	0,407			
1352	0,375	1345	1	naphtalene CCH bend + C=C stretch + C-O-H bend
1386	1	1379	0,543	naphtalene CCH bend + C=C stretch + phenolic C-O-H bend
1418 (broad)	0,787	1398	0,475	naphtalene CCH bend + phenolic C-O bending
1469	0,41	1463	0,237	naphtalene CCH bend + phenolic C-O stretch
1510	0,674	1498	0,074	C=C stretch of naphtalene part + phenolic C-O-H bend
1581	0,791	1564	0,117	C=C stretch of naphtalene part + phenolic C-O-H bend
1612 (broad)	0,633	1616	0,276	C=C stretch of naphtalene part
1637	0,784	1663	0,549	C=O stretch of the COOH group
3066	0,775	3033	0,275	aromatic C-H stretch
3075	0,877	3042	0,373	aromatic C-H stretch
3089	0,46	3062	0,315	aromatic C-H stretch
3230	0,153	3195	0,106	phenolic O-H stretch in intra H bond with C=O
		3572	0,17	O-H stretching of COOH group

Table S5 Assignment for the most characteristic vibrational bands of Caff:1H2N cocrystals.

Experimental Raman shifts	Experimental Raman Normalized Intensity	DFT calculated and corrected Raman shifts	DFT Raman Normalized Intensity	Assignement
293	0,0328	298	0,01	
337	0,103	337	0,08	
353	0,02	353	0,027	
431	0,041	420	0,014	
448	0,064	441	0,023	
494	0,073	490	0,021	
537	0,081	538 (shoulder)	0,08	
563	0,145	545	0,118	
609	0,027	600	0,011	
651	0,031	639	0,012	
725	0,166	722	0,106	
765	0,072	749	0,025	
1028	0,116	1023	0,073	
1083	0,063	1068	0,029	
1155	0,06	1145	0,01	
1208	0,31	1214	0,082	
1263	0,146	1252	0,05	
1298	0,108	1274	0,051	
1374	1	1360	1	imidazole C=N stretch + C-O-H carboxylic group bend bonded by H bonds
1413	0,313	1387	0,043	
1431	0,149	1419	0,038	
1461 (shoulder)	0,171	1455	0,07	
1470	0,219	1465	0,055	
1508	0,174	1495	0,035	
1582	0,148	1586	0,048	
1624 (shoulder)	0,189	1618	0,075	
1647	0,462	1635	0,24	C=O stretch of COOH group bonded by H bond to imidazole group
1662 (shoulder)	0,254	1664	0,054	
1707	0,284	1703	0,065	in phase C=O stretchs of caffeine
2956	0,2	2936	0,415	
2995 (shoulder)	0,116	2992	0,032	
3003	0,138	3002	0,028	
3012	0,114	3013	0,025	
3035	0,123	3028	0,029	
3045	0,143	3041	0,087	
3060	0,272	3050	0,106	
3081	0,138	3072	0,071	
3125	0,05	3117	0,032	
3146	0,066	3131	0,053	

Experiments supporting the mechanism proposed

We have investigated the transfer of caffeine across the interface, when the interface is polarized, by analyzing the content of the organic phase by SEM. Biphasic systems composed of an aqueous phase containing 10 mM of Caff and organic phases with electrolyte salts allowing negative, intermediate and positive polarization of the interface were prepared. A non-polarized biphasic system was also prepared as a control experiment. After 16 h, the organic phase was carefully collected and dropped onto a carbon tape. The solvent was left to evaporate and the samples were metallized with a thin layer of gold (5 nm). SEM images show that large crystals are collected from the organic phase when the interface was positively polarized. When the interface is polarized with an intermediate or a negative potential difference, almost no deposits are observed on the substrate. For the control experiment, i.e. in the absence of polarization, crystals were formed in the organic phase. This, in our opinion, constitutes an indirect proof of caffeine transfer to the organic phase when the interface is positively polarized.

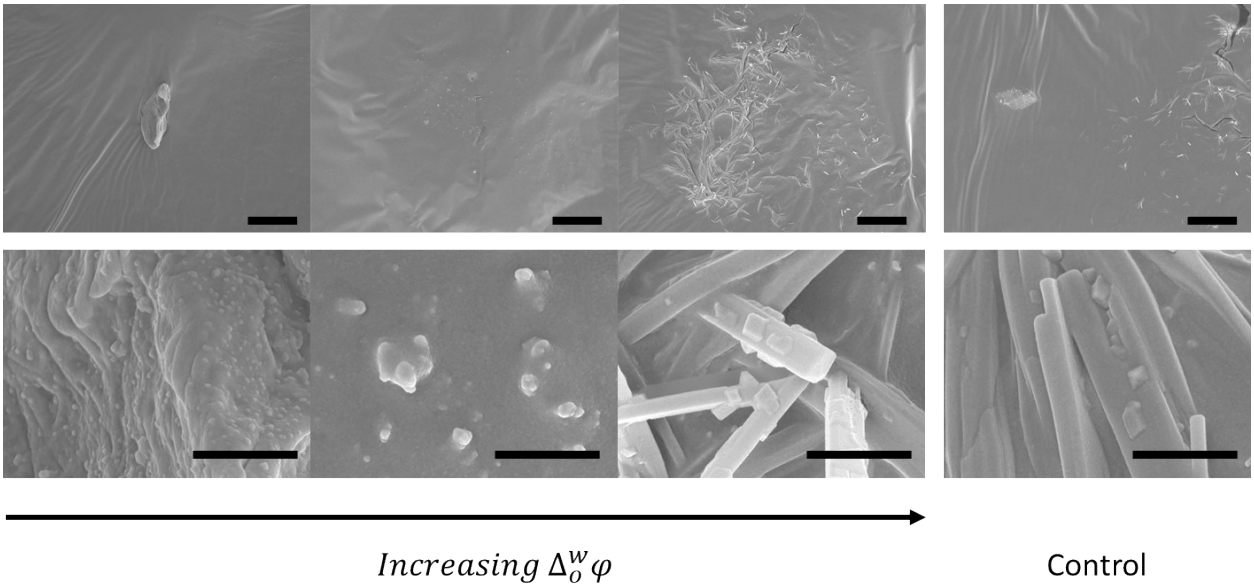

Figure S9: SEM images of the organic phase after solvent evaporation for negative, intermediate and positive polarization of the interface and for control experiments. Top images: scale bars: 20µm; bottom images: 1 µm.

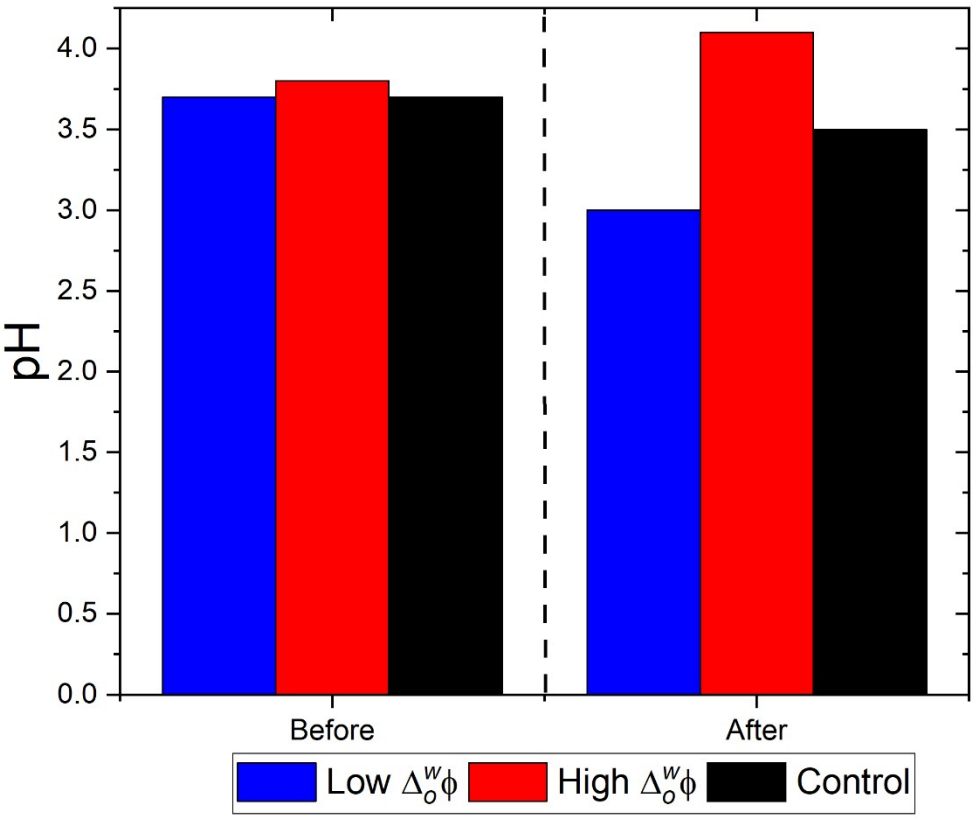

Figure S10: Changes in pH before and after the cocrystallization process for caffeine saturated solution.

References:

[1] V. Chopineaux-Courtois, F. Reymond, G. Bouchard, P. A. Carrupt, B. Testa, H. H. Girault, *J. Am. Chem. Soc.* **1999**, *121*, 1743–1747.

[2] L. J. Sanchez Vallejo, J. M. Ovejero, R. A. Fernández, S. A. Dassie, *Int. J. Electrochem.* **2012**, *2012*, 1–34.

[3] L. Quoc Hung, *J. Electroanal. Chem.* **1980**, *115*, 159–174.

[4] T. Iwata, H. Nagatani, T. Osakai, *Anal. Sci.* **2017**, *33*, 813–819.

[5] L. Poltorak, I. Eggink, M. Hoitink, E. J. R. Sudhölter, M. De Puit, *Anal. Chem.* **2018**, *90*, DOI 10.1021/acs.analchem.8b00916.

[6] P. D. Beattie, R. G. Wellington, H. H. Girault, *J. Electroanal. Chem.* **1995**, *396*, DOI 10.1016/0022-0728(94)03734-K.

[7] C. R. Groom, I. J. Bruno, M. P. Lightfoot, S. C. Ward, *Acta Crystallogr. Sect. B Struct. Sci. Cryst. Eng. Mater.* **2016**, *72*, 171–179.

[8] A. Hédoux, A. A. Decroix, Y. Guinet, L. Paccou, P. Derollez, M. Descamps, *J. Phys. Chem. B* **2011**, *115*, DOI 10.1021/jp112074w.

[9] A. Eşme, *Indian J. Pure Appl. Phys.* **2019**, *57*.

[10] C. Sui, Q. Tu, N. Chen, B. Yan, Z. Lu, Z. Xu, Y. Zhang, *Spectrosc. Lett.* **2018**, *51*, DOI 10.1080/00387010.2018.1501703.

[11] J. Kang, H. Gu, L. Zhong, Y. Hu, F. Liu, *Spectrochim. Acta Part A* **2011**, *78*, 757–762.